HEFAT2014
10th International Conference on Heat Transfer, Fluid Mechanics and Thermodynamics
14 – 26 July 2014
Orlando, Florida

THERMAL INSTABILITY: FROM CAT'S EYES TO DISJOINT MULTIPLE CELLS NATURAL CONVECTION FLOW IN TALL TILTED CAVITIES

Elsa Báez[1] and Alfredo Nicolás[2]
[1] Author for correspondence
Depto. Matemáticas y Sistemas, UAM-C, 01120 México D F, México
E-mail: ebaez@correo.cua.uam.mx
[2]Depto. Matemáticas, UAM- I, 09340 México, D. F., México
E-mail: anc@xanum.uam.mx

ABSTRACT

Thermal viscous incompressible fluid flows, modeled by the unsteady Boussinesq approximation in primitive variables, are solved numerically, by means of a direct projection method, which involves four steps, at each time level: one for the energy equation (temperature step) and three more for the momentum and continuity equations (motion steps). An operator splitting for a second order time discretization is used, taking care of the nonlinear system of equations. The entire process is semi-implicit, which is a common practice. In the temperature step an elliptic problem is solved. In the first motion step, an intermediate velocity is obtained explicitly, considering only one of the three terms of the approximation of the time derivative, and the linear extrapolation of the nonlinear term from the momentum equation; this velocity does not satisfy the incompressibility constraint. In the second step, a new intermediate velocity is computed using an equation that contains another portion of the approximation of the time derivative and the term associated with the pressure. In this step, an additional assumption is incorporated: the new velocity satisfies the incompressibility constraint, such that its projection onto the free divergence subspace is attained. In the third motion step, the final velocity is calculated through an elliptic problem, which contains the last part of the time derivative and the viscous linear term of the velocity. Additionally, in the second step, an elliptic problem is accomplished for the pressure (Poisson equation), complemented with an appropriated Neumann boundary condition obtained by considering the viscous linear contribution in terms of an irrotational part, which is zero due to the incompressibility constraint, and a solenoidal part approximated by linear extrapolation of known values from the two previous time levels. To solve the elliptic problems that result from this process, efficient solvers exist regardless of the space discretization. Natural convection results describing the flow dynamics in tall tilted cavities are shown, which involve from thermal instability known as "cat's eyes" to disjoint multiple cells. To this end, the Rayleigh number Ra and the aspect ratio of the cavity A (A=ratio of the height to the width of the cavity) are fixed to Ra= 11000 and A=16. The thermal instability we are mentioning is obtained varying the angle φ of the cavity from 0° up to 120°.

INTRODUCTION

Many researches have been conducted to study the heat transfer and fluid flow by natural convection due to their wide engineering applications, such as solar collectors, heat exchangers, cooling of electronic devices, building ventilation and insulation of nuclear reactors, among others. Formulations in terms of primitive (velocity and pressure) [1] and / or secondary (stream function and vorticity) [2,3] variables have been considered to model this problem and solve the equations that describe it. In any case, it must face the nonlinearity and the coupling of these equations. The formulation with primitive variables allows to study problems in three dimensions, but presents some drawbacks as no information about the pressure and it is not easy to satisfy the continuity equation. On the other hand, the formulation in secondary variables, eliminates these inconveniences because the term associated with the pressure disappears and the continuity equation is satisfied automatically, however it is only possible to consider bi-dimensional flows.

In this paper, we use a formulation in primitive variables and a projection scheme, which is based on an operator splitting, to solve the mathematical model. An essential step for the solution of the problem is the way the pressure is solved, through a Poisson equation and an appropriate boundary condition obtained from de momentum equation [4, 5]. The scheme used requires no iteration, it is independent of the dimension of space and the region in which the flow occurs and can be applied to problems in two and three dimensions.

The numerical scheme had been already used by us in other paper, [1], and in this case we apply it to study the effect that the angle of inclination of the cavity has on the pattern of the

flow and on the heat transfer. Validation of the results shown in this paper is made through comparison with those obtained in [2], which in turn were validated by mesh size and time-step independent studies.

MATEMATHICAL MODEL

Natural convection of an unsteady viscous incompressible fluid flow, confined in a rectangular cavity, can be modelled by the Boussinesq approximation through the following system of dimensionless equations, in the domain $\Omega = (0,1) \times (0, A)$, where A is the aspect ratio of the cavity (ratio of the height to the width) whose boundary is denoted by Γ, and $t > 0$:

$$(\mathbf{1}) \quad \begin{cases} \text{a)} \quad \theta_t - \dfrac{1}{\mathrm{Pr}}\nabla^2\theta + (\mathbf{u}\cdot\nabla)\theta = 0 \\ \text{b)} \quad \mathbf{u}_t - \nabla^2\mathbf{u} + \nabla p + (\mathbf{u}\cdot\nabla)\mathbf{u} = \dfrac{\mathrm{Ra}}{\mathrm{Pr}}\,\theta\,(\sin\varphi, \cos\varphi) \\ \text{c)} \quad \nabla\cdot\mathbf{u} = 0 \end{cases}$$

Variables θ, p and $\mathbf{u}$ represent, respectively the temperature, pressure and velocity vector. The parameters Ra y Pr correspond to the Rayleigh and Prandtl numbers, and φ is the angle of inclination of the domain. The continuity equation (1.c) is also known as the incompressibility condition.

The corresponding initial and boundary conditions, that complement this mathematical model are given by

initial conditions: $\theta = 0$ and $\mathbf{u} = \mathbf{0}$ in Ω,

boundary condition: $\theta = 1$ on $\Gamma|_{x=0}$,

$\theta = 0$ on $\Gamma|_{x=1}$,

$$\frac{\partial\theta}{\partial y} = 0 \quad \text{on } \Gamma|_{y=0\,,A}.$$

From the foregoing, it follows that the left wall of the cavity is hot, and the right one is cold; the horizontal walls are insulated. Fluid starts from rest and it has the same temperature than the cold one

To deal with the inherent difficulties of this system of equations, as the coupling among them and the non-linearity, a strategy that combines a semi-implicit discretization in time and a projection method is used.

NUMERICAL SCHEME

Once the time discretization is performed, by means of following second order approximation

$$f_t(\boldsymbol{x}, (n+1)\Delta t) \approx \frac{\frac{3}{2}f^{n+1} - 2f^n + \frac{1}{2}f^{n-1}}{\Delta t}, \quad n \geq 1, \ \boldsymbol{x} \in \Omega$$

and using a projection method to the momentum and continuity equations we must solve in Ω, at each time level, firstly the energy equation to obtain θ^{n+1}:

Temperature step:

$$\left(\nabla^2 - \frac{3}{2\mathrm{Pr}}\right)\theta^{n+1} = 2(\mathbf{u}\cdot\nabla\theta)^{n+1} + \frac{1}{2\Delta t}\theta^{n-1}$$

$$B\theta^{n+1}|_\Gamma = 0$$

where the boundary condition for temperature is involved in the operator B. Next, applying an operator splitting of three steps to equations (1.b) and (1.c), we get the pressure p^{n+1} and the velocity $\mathbf{u}^{n+1}$:

Motion steps:

1)

$$\frac{\mathbf{u}^* - 2\mathbf{u}^n + \frac{1}{2}\mathbf{u}^{n-1}}{\Delta t} = -(\mathbf{u}\cdot\nabla\theta)^{n+1} + \frac{\mathrm{Ra}}{\mathrm{Pr}}\theta^{n+1}(\sin\varphi, \cos\varphi)$$

2)

$$\frac{\mathbf{u}^{**} - \mathbf{u}^*}{\Delta t} = -\nabla p^{n+1}$$

$$\nabla\cdot\mathbf{u}^{**} = 0$$

3)

$$\frac{\frac{3}{2}\mathbf{u}^{n+1} - \mathbf{u}^{**}}{\Delta t} = \nabla^2\mathbf{u}^{n+1}$$

$$\mathbf{u}^{n+1}|_\Gamma = \mathbf{0}$$

The intermediate velocity $\mathbf{u}^*$, obtained in the first motion step, is projected onto the space of divergence free and thus, in step 2, the second intermediate velocity $\mathbf{u}^{**}$ satisfy the incompressibility condition; at the end, the final velocity $\mathbf{u}^{n+1}$ is calculated in step 3.

Some remark must be made regarding the above steps:

a) the nonlinear convective terms are approximated by a linear extrapolation from the respective values of θ and $\mathbf{u}$ at time levels n and n-1.

b) To obtain the pressure p^{n+1}, required in the equation of step 2, the divergence of this equation is considered and taking into account that $\mathbf{u}^{**}$ is divergence free, a Poisson equation for the pressure is attained [4, 5]

$$\nabla^2 p^{n+1} = \frac{1}{\Delta t}\nabla\cdot\mathbf{u}^*,$$

a suitable boundary condition is accomplished by taking the normal component of the semi-discrete momentum equation, where $\nabla^2\mathbf{u}$ is described in terms of a irrotational part [5], which is zero due equation (1.c), and another solenoidal ($\nabla^2\mathbf{u} = \nabla(\nabla\cdot\mathbf{u}) - \nabla\times(\nabla\times\mathbf{u})$), which is approximated through an linear extrapolation of the values at two previous times levels

$$\frac{\partial p^{n+1}}{\partial \mathbf{n}} = \mathbf{n}\cdot\left[\frac{1}{\Delta t}\left(-\frac{3}{2}\mathbf{u}^{n+1}+2\mathbf{u}^{n}-\frac{1}{2}\mathbf{u}^{n-1}\right)-2\left((\mathbf{u}\cdot\nabla\mathbf{u})^{n}+\nabla\times(\nabla\times\mathbf{u}^{n})\right)+\left((\mathbf{u}\cdot\nabla\mathbf{u})^{n-1}\right)+\nabla\times(\nabla\times\mathbf{u}^{n-1})+\frac{Ra}{Pr}\,\theta^{n+1}(\sin\varphi,\cos\varphi)\right)\quad \text{on } \Gamma.$$

Some detail of the numerical scheme can be seen in [1]. Thus, at each time level three elliptic problems must be solved to find θ^{n+1}, p^{n+1}, $\mathbf{u}^{n+1}$ and several solvers exist for this kind of problems, regardless of the spatial discretization. For this purpose, we use the second order finite difference approximations of the Fishpack solver [6]

After temperature θ and final velocity $\mathbf{u} = (u_1, u_2)$ are obtained, the heat transfer on the hot wall can be computed by means of Nusselt numbers, local Nu(y) and global $\overline{Nu}$, as well as the vorticity ω and the stream function ψ in Ω:

$$Nu(y) = \left.\frac{\partial\theta}{\partial x}\right|_{x=0} \qquad \text{and} \qquad \overline{Nu}|_{x=0} = \frac{1}{A}\int_0^A \mathrm{Nu(y)dy}$$

$$\omega = \frac{\partial u_2}{\partial x} - \frac{\partial u_1}{\partial y}$$

$$\nabla^2\psi = -\omega$$

NUMERICAL RESULTS

Some numerical results for natural convection are shown for a rectangular cavity with aspect ratio A=16, and filled with air, Pr=0.71. A specific value of Rayleigh number, Ra =11000, and angles 0º ≤ φ≤ 120º are considered. Only flows that have reached the steady states are reported, which is determined by the point-wise discrete L_∞ absolute criterion in the closure $\bar{\Omega}$, applied to θ and **u.**

$$\left\|\theta^{n+1}_{hx,hy} - \theta^{n}_{hx,hy}\right\|_\infty < tol$$

$$\left\|\mathbf{u}^{n+1}_{hx,hy} - \mathbf{u}^{n}_{hx,hy}\right\|_\infty < tol$$

with *tol* = 10^{-5}. The results were obtained using a mesh size given by $h_x \times h_y = \frac{1}{24}\times\frac{16}{384}$ and a time step Δt = 10^{-4}. They are presented in terms of temperature (isotherms), stream function (streamlines) and the local Nusselt number. These are complemented with values, maxima and minima, of ψ and of the velocities $u_1$and u_2, the time T_{ss} where the steady state is reached, $\overline{Nu}$ and the number of cells that appear in the streamlines.

Results for φ = 0º, Figure 1, show one primary cell in the streamlines, however three secondary cells appear along of the center of the cavity; these instabilities are also called cat's eyes (cey). The isotherms are distorted in the regions where these sub-cells appear. The local Nusselt number on the hot wall, Figure 4, indicates that the maximum heat transfer occurs on the bottom of this wall, and from ψ_{min} / ψ_{max} values in Table 1 follow that the single main cell and secondary cells rotate clockwise.

When φ = 40º, Figure 2, an additional secondary cell arises, then there are four cat's eyes in the streamlines, and all of them have increased their size; as in the previous angle, the isotherms also show an increase in distortions, according to the number of cells in the streamlines. The respective graphic of local Nusselt number shows that even though the heat transfer has a maximum in the bottom of the hot wall, there are three more maxima, which is due to the effect of secondary cells. Values registered in Table 1 and 2 indicate that the fluid rotates clockwise, but its motion is slower, and the heat transfer (measured by $\overline{Nu}$) is lower, however the time to reach the steady state is greater than that obtained for φ = 0º.

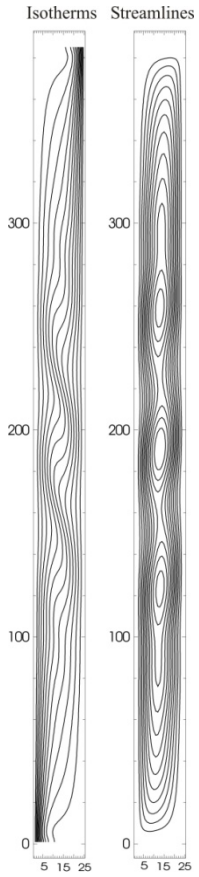

Figure 1 Isotherms and streamlines for A=16 and φ = 0º

φ	ψ_{min}/ψ_{max}	$\overline{Nu}$	Cells
0º	-37.8486 / 0.0	1.5351	3(cey)
40º	-30.4225 / 0.0	1.4804	4(cey)
60º	-20.2692 / 8.0485	1.9699	5
90º	-13.6032 / 13.7991	2.7944	19
120º	-7.9668 / 20.2405	1.9710	5

Table 1 Numerical results for A=16 and several angles φ

φ	$u_{1\,min}$/ $u_{1\,max}$	$u_{2\,min}$/ $u_{2\,max}$	T_{ss}
0º	-19.3557 / 19.3348	-123.0505 / 123.2267	1.7645
40º	-19.5678 / 19.5234	-98.0422 / 98.4124	2.8061
60º	-22.1005 / 23.4810	-64.4653 / 64.5229	3.0752
90º	-51.4627 / 51.4442	-44.6598 / 44.7194	0.6693
120º	-22.1292 / 23.1400	-64.5297 / 64.4176	3.9932

Table 2 Continuation.

For φ > 40º, the secondary cells increase their size as the angle does, up to some angle 40º < φ* < 60º where the pattern changes to multiple disjoint cells (multi-cellular flow). the number of these disjoint cells also increases with the angle and this new pattern holds up to φ = 90º (heating from below), shown in Figure 3. As indicated in Table 1, when φ = 60º there are 5 main cells in the streamlines, while for φ = 90º a total of 19 main cells appear, in these cases adjacent main cells rotate in opposite directions. The ridges and valleys appearing on the isotherms, in Figure 3, correspond to the regions where the cells carry the cold fluid to the hot wall, and viceversa. The first ones are also associated with the respective maxima in the graphic of the local Nusselt number, and the second ones with the minima. Furthermore, from Tables 1 and 2, the fluid motion is stronger and the time T_{ss} is higher when φ = 60º that those when φ = 90º, but the heat transfer is greater for this last angle.

Figure 2 Isotherms and streamlines for A=16 and φ = 40º

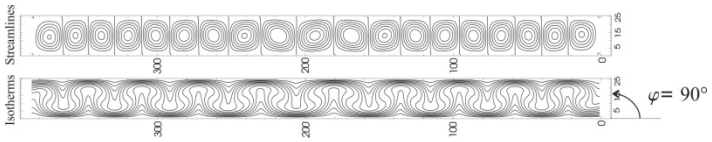

Figure 3 Isotherms and streamlines for A=16 and φ = 90º

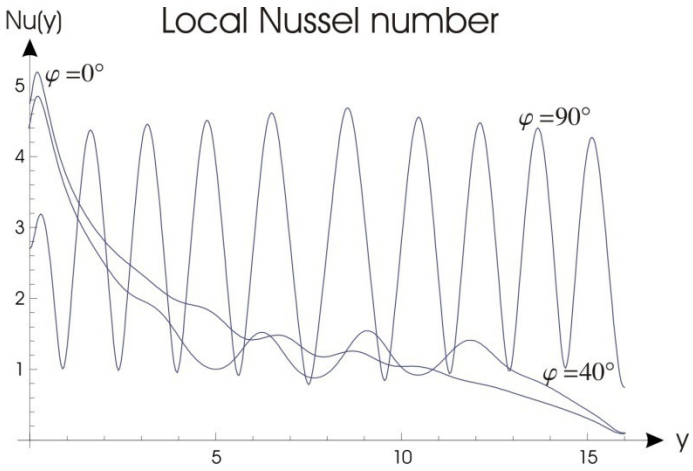

Figure 4 Local Nusselt number for A=16 and φ = 0º, 40º, 90º

Remark: the difference in size of the graphs of Figure 3, with respect to those of Figures 1 and 2, is due to the margins of the template.

The pattern described in the preceding paragraph seems to repeat itself, but in the reverse direction, as the angle continues to increase from φ = 90º, this means that when the angle increases, the number of main cells decreases up to only get one, in which secondary cells appear along of it, until φ = 180º. An example of this situation is shown in Table 1 and Table 2, where it can be observed that values obtained for φ = 120º are very similar to those obtained for φ = 60º, but several of them are interchanged, which is due to the symmetrical position of the cavity for both angles, and therefore the reverse motion of the fluid respect to the φ = 60º.

Results shown here are consistent with those in [2], for A = 16, where formulation with temperature and secondary variables (stream function and vorticity), as well as the same data, were used. Characteristics of the respective graphs of the stream function and temperature, as the number of cells (secondary or disjoint) and distortion, are identical in both formulations. The values of the magnitudes obtained in the two papers have a difference less than 3.2%. It can be seen that, for all angles shown here, the time T_{ss} to reach the steady state is higher in secondary formulation variables, and this difference is more pronounced for angles where multiple disjoint cells appear.

The results obtained in this paper indicate that:

a) fluid motion is stronger for lateral heating ($\varphi = 0º$),
b) the higher heat transfer happened when the heating is from below,
c) φ^* is the angle when the transition, when flow changes from unicellular to multicellular, and $40º < \varphi^* < 60º$,
d) the greatest number of disjoint cells (19) in the streamlines happens when $\varphi = 90º$,
e) the characteristics and values of fluid flow for angles $90º < \varphi \leq 120º$ are very similar, by symmetry, to their equivalent when $90º > \varphi \geq 60º$, but fluid motion is reverse,
f) for those angles when thermal instabilities (cat's eyes or secondary cells) appear, the highest heat transfer occurs when $\varphi = 0º$; something similar happens for those angles when disjoint cells are obtained, where the highest heat transfer is reached when the heating is from below ($\varphi = 90º$).

CONCLUSION

Numerical results for fluid flow by natural convection, in a rectangular cavity filled with air, are obtained for specific values of $Ra=1.1 \times 10^{-4}$ and A= 16 and several angles φ ($0º \leq \varphi \leq 120º$), using a projection method of four steps,. The results indicate that, when the heating is lateral the flow is unicellular, and some thermal instabilities are present. This pattern continues until a transition angle $40º < \varphi^* < 60º$, from which multi-cellular flow is obtained. The presence of multiple cells, primary or secondary, contribute to transport the fluid from the cold to the hot wall, and viceversa, and increase the heat transfer in various parts of the hot wall. The fluid motion is stronger for lateral heating ($\varphi = 0º$), but higher heat transfer happens when the heating is from below ($\varphi = 90º$). Moreover, a considerable increase in the time T_{ss} to reach the steady state is observed in those cases where the angle φ is closer to the transition angle φ^*.

REFERENCES

[1] Báez E., Nicolás A., From cat's eyes to multiple disjoint natural convection flow in tall tilted cavities: A direct primitive approach, *Phys. Let. A,,* Vol. 377, 2013, pp. 2270-2274.

[2] Nicolas A., Báez E. Bermúdez B. From cat's eyes to disjoint multicellular natural convection flow in tall tilted cavities. *Phys. Let. A,* Vol. 375, 2011, pp. 2683-2688.

[3] Báez E. and Nicolás A. 2D Natural Convection Flows in Tilted Cavities: Porous Media and Homogeneous Fluids. *Int. J. of Heat and Mass Transfer* Vol. 49 , No, 25, 2006, pp. 4773-4785.

[4] Sani R. L., Shen J., Pironneau O., Gresho P. M. Pressure boundary condition for the time-dependent incompressible Navier-Stokes equations. *Int. J. Num .Meh. in Fluids,* Vol. 50, 2006, pp. 673-682.

[5] Karniadakis G. E. Israeli M. And Orszag, S. A. Hilgh-order splitting methods for the incompressible Navier-Stokes equations, *Journal of Comp. Phys.*, Vol. 97, 1991, pp. 414-443.

[6] Adams J., Swarztrauber P. and Sweet R., FISHPACK: A Package of Fortran Subprograms for the Solution of Separable Elliptic PDE's, *The National Center for Atmospheric Research*, Boulder, Colorado, 1980.